

Chemical ordering and composition fluctuations at the (001) surface of the Fe₆₄Ni₃₆ Invar alloy

M. Ondraček, F. Mica, and J. Kudrnovský

Institute of Physics ASCR, Na Slovance 2, CZ-182 21 Praha 8, Czech Republic

J. Redinger

Center for Computational Materials Science, Getreidenarkt 9/134, A-1060 Vienna, Austria

A. Biedermann

Institut für Materialphysik, University of Vienna, Strudlhofgasse 4, A-1090 Vienna, Austria

C. Fritscher,^y M. Schmid, and P. Varga

Institut für Allgemeine Physik, Vienna University of Technology,
Wiedner Hauptstr. 8-10, A-1040 Vienna, Austria

(Dated: November 13, 2006)

We report on a study of (001) oriented fcc Fe-Ni alloy surfaces which combines first-principles calculations and low-temperature STM experiments. Density functional theory calculations show that Fe-Ni alloy surfaces are buckled with the Fe atoms slightly shifted outwards and the Ni atoms inwards. This is consistent with the observation that the atoms in the surface layer can be chemically distinguished in the STM image: brighter spots (corrugation maxima with increased apparent height) indicate iron atoms, darker ones nickel atoms. This chemical contrast reveals a c(2 × 2) chemical order (50% Fe) with frequent Fe-rich defects on the Fe₆₄Ni₃₆ (001) surface. The calculations also indicate that subsurface composition fluctuations may additionally modulate the apparent height of the surface atoms. The STM images show that this effect is pronounced compared to the surfaces of other disordered alloys, which suggests that some chemical order and corresponding concentration fluctuations exist also in the subsurface layers of Invar alloy. In addition, detailed electronic structure calculations allow us to identify the nature of a distinct peak below the Fermi level observed in the tunneling spectra. This peak corresponds to a surface resonance band which is particularly pronounced in iron-rich surface regions and provides a second type of chemical contrast with less spatial resolution but one that is essentially independent of the subsurface composition.

PACS numbers: 73.20.-r, 68.37.Ef, 73.61.At

Keywords: nickel; iron; alloy; surface electronic structure; scanning tunneling microscopy; density functional calculations

I. INTRODUCTION

The properties of alloy surfaces are of great importance for surface- and interface-related phenomena like segregation and catalysis, furthermore, examination of the surface makes it possible to study bulk properties not easily accessible by other methods. Scanning tunneling microscopy (STM) and spectroscopy (STS) have become indispensable methods for imaging alloy surfaces^{1,2,3,4} and surface alloys^{5,6,7} with atomic resolution and chemical contrast. This paper focuses on the interpretation of STM/STS data of a transition metal alloy, the Fe₆₄Ni₃₆ alloy, based on first-principles calculations. In the course of this analysis two separate modes of chemical contrast in STM images are discussed: First, apparent height differences of different chemical species providing chemical contrast in an atom-by-atom fashion; Second, chemical contrast based on specific features of the tunneling spectra, in particular surface state peaks.

On many transition metal surfaces, surface states and resonances near the Fermi level have been detected by STS^{8,9,10,11,12,13}. However, according to experience and the most basic theory of the STM¹⁴ only a small fraction

of surface states, specifically those which are sufficiently delocalized perpendicular to the surface, can be seen by the STM, i.e., contribute to the tunneling current. A class of surface resonances accessible by STS is that with s-p_z-d_{z²} symmetry at the $\bar{\Gamma}$ -point observed on the bcc(001) surfaces of Fe⁹, Cr¹¹, V¹³, W¹⁵, and their surface alloys Cr-Fe¹¹ and Si-Fe¹², and on the hcp(0001) surface of Gd/W(110)¹⁶. These states may serve as an extra source of chemical contrast as alloy components tend to locally quench the surface resonance as demonstrated for the dilute surface alloy Cr/Fe(001)¹¹ and the chemically ordered surface alloy Si/Fe_{96.4}Si_{3.6}(001)¹².

In this article we apply these ideas to the fcc alloy surface Fe₆₄Ni₃₆(001) which is different from the mentioned surface alloys in at least two ways: (1) Subsurface composition fluctuations^{7,18} lead to relatively strong variations of the apparent height of the surface atoms on the nanometer scale, which makes the chemical assignment of the individual atoms, successfully done for the alloy surfaces Pt₂₅Ni₇₅(111)¹ or Pt₅₀Rh₅₀(001)⁴, rather difficult. (2) This surface does not show clusters or chains of Fe or Ni atoms which a priori could be considered sufficiently large to support 1D or 2D surface resonances

characteristic for the elements constituting the alloy.

$\text{Fe}_{64}\text{Ni}_{36}$ has a very low thermal expansion for temperatures up to its Curie temperature of approximately 500 K and is therefore known under the trademark Invar since its discovery more than 100 years ago. Invar and other iron-rich Fe-Ni alloys are applied in numerous thermally stabilized or matched components. The thermal anomalies of these materials are explained by a temperature dependent atomic volume of Fe in the ferromagnetic state counteracting "regular" thermal expansion due to lattice anharmonicity (cf., e.g., Refs. 17,19,20). A non-collinear magnetic ordering has been predicted¹⁷ and observed recently²¹, which depends on composition fluctuations and chemical order^{17,18,22}. Therefore, local properties like chemical order, surface and subsurface composition, and surface electronic structure are very relevant to deepen the understanding of this technologically important system.

After presenting the experimental results, we first investigate the surface geometry of Fe-Ni(001) alloys from first-principles, in particular, we will demonstrate that the alloy surface is buckled and this buckling allows us to explain the chemical contrast observed in atomically resolved STM images. Second, we present a detailed first-principles investigation of the surface electronic structure of the $\text{Fe}_{64}\text{Ni}_{36}$ (001) alloy surface and show that the surface resonance found just below the Fermi level of Fe-rich surfaces is in accordance with the local spectroscopic features found in the STM experiment.

II. EXPERIMENT

A. Setup and sample preparation

The experiments were done using a low-temperature scanning tunneling microscope (LT-STM) mounted inside of cryo-shields cooled by a bath cryostat filled with liquid N_2 or liquid He (Omicron LT-STM). The microscope is operated with electrochemically etched W tips conditioned by sputtering with Ar^+ under ultrahigh-vacuum (UHV) conditions. The LT-STM system is equipped with an Auger electron spectroscopy (AES) system for a surface sensitive chemical analysis. A separate UHV chamber was used for low energy electron diffraction (LEED) measurements at 300 K and above to probe the temperature dependence of the surface chemical order. The pressure during measurement in the separate STM chamber of the LT-STM system is around $1 \cdot 10^{-11}$ mbar, and in the chamber with the LEED system in the 10^{-11} mbar range.

The $\text{Fe}_{64}\text{Ni}_{36}$ (001) single crystal was typically prepared by sputtering with 2 keV Ar^+ ions and subsequent annealing at 770 K for 10 minutes.

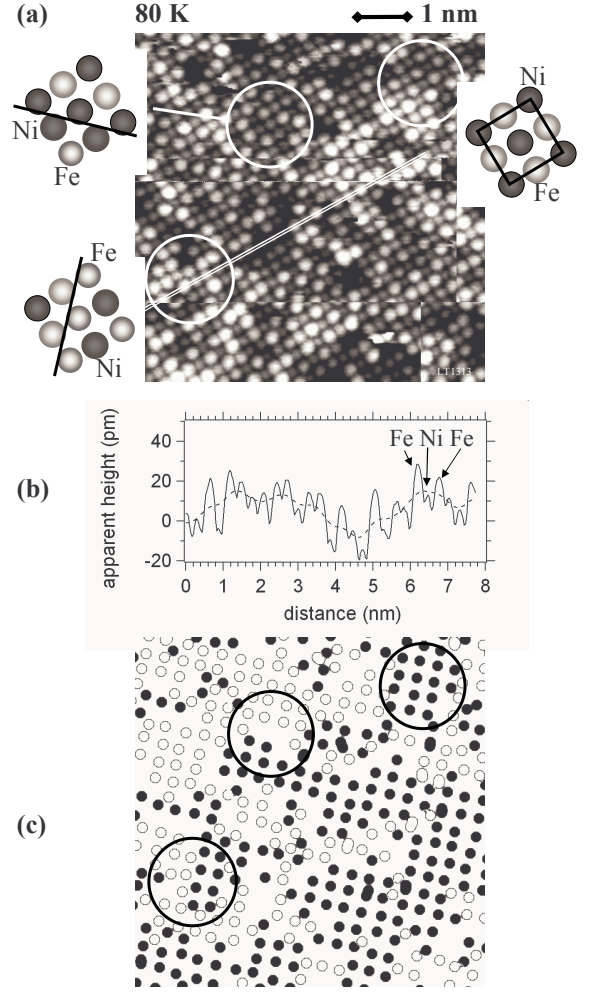


FIG. 1: (a) STM image of the $\text{Fe}_{64}\text{Ni}_{36}$ (001) surface (sample voltage -2 mV, tunneling current 8 nA). The three details highlight a (2×2) -ordered area (unit cell marked by square) and both a short Ni-rich and a short Fe-rich antiphase domain boundary segment. (b) Profile of the STM image along the white line in (a). The dashed average curve indicates a long-wavelength buckling on the nanometer scale in contrast to the short-wavelength buckling distinguishing Fe and Ni atoms. (c) Map of automatically detected Fe atom locations (cornugation maxima) in the STM image omitting the Ni atoms, with each of the Fe atoms assigned to one of the two (2×2) antiphase sublattices (open and full circles, occasional oval shapes are due to the detection of more than one cornugation maximum per atom caused by image errors).

B. Chemical contrast and surface order

Figure 1 shows an STM image of the $\text{Fe}_{64}\text{Ni}_{36}$ (001) surface at 80 K. The distinctly different brightness (apparent height) of adjacent atoms indicates a chemical contrast between Fe and Ni atoms. Images from similar $\text{Fe}_{64}\text{Ni}_{36}$ surfaces covered by additionally deposited Fe

(about 1 monolayer) in order to artificially increase the Fe content suggest that the "dark" species is Ni. This atom-by-atom chemical contrast reveals that the surface is locally ordered with a $c(2 \times 2)$ superstructure [top right detail in Fig. 1(a)]. Since the Fe surface concentration is higher than 50% (cf. next paragraph), the excess Fe has to be inserted as Fe-rich defects, which often are short pieces of Fe-rich anti-phase domain boundaries (bottom left detail). Occasionally, however, also Ni-rich defects are visible in the STM images (middle detail), indicating that the disorder is larger than required to accommodate the excess Fe. A LEED experiment probing the temperature dependence of the $(1/2, 1/2)$ -type superstructure spots normalized to $(1, 0)$ integer spots shows a reversible rather abrupt disappearance and reappearance of the signal near 550 K indicating an order-disorder transition there. Atomically resolved STM images with up to 20×20 nm frame size suggest typical anti-phase domain diameters between 1 and 10 nm at 80 K.

The chemical analysis by automatically counting bright and dark atoms based on their apparent height is very unprecise (46% \pm 12% Ni) since the histogram of apparent atom height values does not show a clear bimodal distribution of dark and bright atoms. The reason is a significant buckling of the surface in the entire spatial wavelength range of the image [dashed line in Fig. 1(b)], interfering with the buckling providing the chemical contrast between adjacent atoms. Only strong high pass

filtering (not shown in Fig. 1), leaving only height differences of adjacent atoms in the image, leads to separable peaks in the histogram of apparent atom heights, which can be fitted by a double gaussian. Combining the resulting Ni concentration with results from manual atom counting and a quantitative AES analysis, using the surface sensitive low-energy peaks of Fe and Ni, results in a Ni concentration of 41% with an estimated error of \pm 2% for the annealed $\text{Fe}_{64}\text{Ni}_{36}$ surface | a small Ni enrichment relative to the nominal bulk concentration of 36%.

The buckling of the surface layer on the nanometer scale may be explained by the subsurface distribution of larger Fe and smaller Ni atoms. Since there exists no long-range order in the $\text{Fe}_{64}\text{Ni}_{36}$ bulk, the first hypothesis assumes a fully random order of the subsurface Fe and Ni atoms, which implies random composition fluctuations. However, the surfaces of the disordered alloy $\text{Pt}_{25}\text{Ni}_{75}$ (111)¹, which show weak surface order, or of the alloy $\text{Pt}_{25}\text{Rh}_{75}$ (100)³ do not show a comparable surface buckling on the nanometer scale. Therefore most likely the second hypothesis applies which assumes subsurface local order as observed in the $\text{Fe}_{64}\text{Ni}_{36}$ bulk by element specific x-ray scattering experiments¹⁸. This would be an arrangement of subsurface Fe and Ni atoms which is rather similar to that seen on the surface with $c(2 \times 2)$ ordered regions (50% Fe) interrupted by frequent small Fe-rich domain boundary fragments. The corresponding composition fluctuations would then have a characteristic length scale above 1 nm, i.e., the diameter of Fe-rich defects or ordered domains, as observed, while fluctuations

in randomly distributed alloys are strong only at very local scales, which have less influence on the buckling of adjacent atomic layers. We remark, however, that it is likely that the chemical order on the surface is higher than that in the subsurface layers due to smaller barriers for atom exchange on the surface and the low order-disorder transition temperature of the system around 550 K, i.e., a temperature which seems prohibitive for efficient bulk diffusion (assuming equal transition temperatures for the surface and the bulk).

As mentioned at the beginning of this section, this convolution of surface and subsurface effects make the chemical analysis of the surface based on apparent atom heights rather cumbersome. In addition, in many cases the STM images do not show the individual metal atoms and the brightness variations cannot be unambiguously assigned to either surface chemical contrast or surface buckling. However, tunneling spectroscopy may be used to separate surface and subsurface effects (although with less spatial resolution and less precision as demonstrated in the next section).

C. Chemical contrast by scanning tunneling spectroscopy

Figure 2 shows STS images and tunneling spectra of the $\text{Fe}_{64}\text{Ni}_{36}$ (001) surface at 5 K and spectra only for a surface at 80 K. Data acquisition was done by measuring I/V curves for every image point with the tip position z_0 adjusted to 1 nA at -1 V tunneling voltage in every image point [Fig. 2(a)], followed by numerical differentiation. The spectra shown in Fig. 2(c) are averages over a few tens of individual spectra from equivalent image points of the same STS image without additional smoothing. Both experiments, 5 and 80 K, show a distinct peak at 0.35 \pm 0.1 eV below the Fermi edge, which is intense, however, only in a very small fraction of the surface. The

first principles calculations in the following sections will describe the character of the underlying electronic states in detail. In this section we will use the term "surface resonance peak" for the sake of simplicity. The small peak shift of 0.1 eV between 5 and 80 K is not significant within the precision of this measurement. The small peak visible in the 80 K measurement [arrow in Fig. 2(a)], appears in the spectrum of every image point in this data set only, which is characteristic for a tip-related state.

The peak shape is rather symmetric, indicating little dispersion of that part of the surface resonance band that is visible for the STM (cf. Sect. IIIB). The width (FWHM) is about 250 meV, which is quite large compared to similar peaks on the $\text{Cr}(001)$ ²³ or $\text{Gd}(0001)$ ¹⁶ surface at 5 K. However, it is comparable to the width of the resonance of single Fe atoms on the $\text{Pt}(111)$ surface at 5 K (\sim 300 meV)²⁴. The calculations in the next sections show that the peak can indeed be assigned to Fe-rich defects on the chemically ordered $\text{Fe}_{64}\text{Ni}_{36}$ (001) surface.

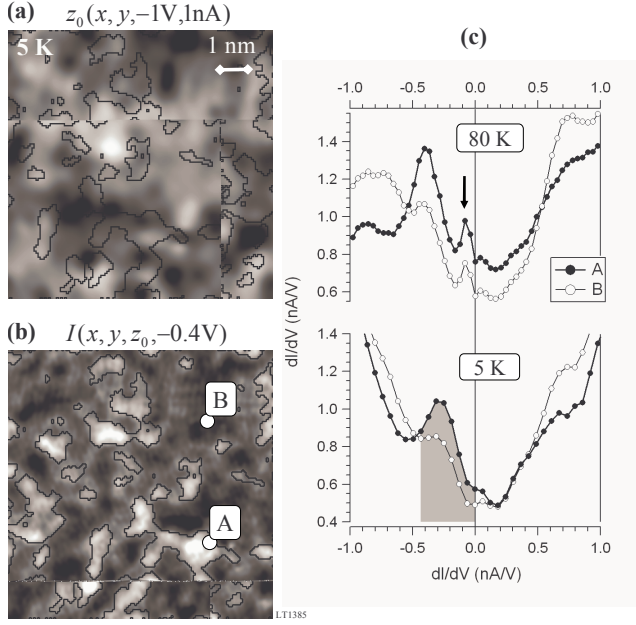


FIG. 2: (a) Constant current image of the $\text{Fe}_{64}\text{Ni}_6$ (001) surface at 5 K, 1 nA tunneling current, and -1 V sample voltage. (b) Corresponding current map at -0.4 V, showing the intensity of a surface resonance below the Fermi-level (shaded area in 5 K spectrum to the right). (c) dI/dV (V) spectra at 5 K corresponding to the images at left and of a separately prepared sample at 80 K. Shown are spectra near extremal points of the surface resonance intensity, both for maximum (A) and minimum (B) intensity. The small peak at -0.1 V in the 80 K spectra is a tip-related state (arrow). The contour lines in (a) and (b) encompass the relatively small surface fraction that shows spectra which are more similar (smaller root mean square deviation) to spectrum A than to spectrum B. The remaining larger surface fraction shows spectra which are more similar to spectrum B. Evidently, the surface fraction with significant surface resonance intensity is rather small (26% in this data set) consistent with the assumption that it marks Fe-rich regions.

Mapping the tunneling current at a voltage just below the low-energy edge of the resonance peak by plotting $I(x, y; z_0; -0.4 \text{ V})$ from the complete I/V dataset provides a map of the surface resonance intensity acquired in a distance of more than 0.5 nm from the surface plane [Fig. 2 (b)]. By evaluating the similarity of the spectrum in each image point to the peaked spectrum (A) and the "flat" spectrum (B) we find (see caption Fig. 2) that the surface resonance peak is a minority property of the surface, with the larger surface fraction showing no or only a small peak, suggesting a correlation to the Fe-rich defects seen in the atomically resolved images [Fig. 1 (a)]. Direct comparison of the classification by the tunneling spectra [contours in Fig. 2 (a,b)] with the constant current image [Fig. 2 (a)] demonstrates that the apparent

height of the surface does not obviously correlate with the map of the surface resonance intensity. Although a weak correlation should exist, because the composition of the surface monolayer contributes to the apparent height as well, it is too weak to be relevant compared to the height variation caused by the compounded effect of concentration inhomogeneities in each of several monolayers below the surface monolayer. Thus, the tunneling spectra provide a method to map the chemical information independent of the geometric height information on every image scale without the requirement to resolve the surface atomically. We remark that, although desirable, it would be extremely difficult to combine such a spectroscopic analysis with the simultaneous acquisition of an atomically resolved image, mainly due to the instability and short lifetime of very sharp tips.

III. DFT CALCULATIONS

A. Surface relaxation

We first investigate the surface geometry of the Fe-Ni alloy. The relation between crystal structure and magnetic ordering is of crucial importance for iron-based alloys. The calculations have been done using the full-potential linearized augmented plane wave method²⁵ (FP-LAPW) code FLAIR²⁶. Two approximations for the density functional potential have been used: the local density approximation (LDA) according to Vosko, Wilk, and Nusair²⁷ and the generalized gradient approximation (GGA) according to Perdew, Burke and M. Ernzerhof²⁸. Spherical wave and plane wave expansions were truncated at $l_{\text{max}} = 8$ and $E_{\text{cut}} = 11.6 \text{ Ry}$ respectively. The difference between the last two charge density iterations was less than 10^{-6} e.a.u.^3 . In all the surface geometry optimizations, atomic positions in the surface and two subsurface layers were fully relaxed²⁹. The final relaxed structure was assumed when the force on each atom was smaller than 5 meV/\AA . Nine-layer ordered films have been used to simulate fcc(001) alloy surfaces with different ordering. For all the calculations we have used the experimental lattice constant $a = 3.58 \text{ \AA}$ ³⁰. Minimizing the total energy as a function of lattice constant for a NiFe_3 crystal yields the value $a = 3.60 \text{ \AA}$. Our model geometries are derived from a NiFe_3 (001) surface structure composed of $c(2 \times 2)$ NiFe (001)-layers alternating with pure Fe (001) layers. It should be noted here that this corresponds to the Cu_3Au structure, also known as L1_2 . Our models are in accordance with STM experiments, which indicate approximately the same amount of iron and nickel atoms in the top surface layer. All model systems exhibit inversion symmetry and include 18 atoms in the unit cell. Some models have only iron atoms in the subsurface layer and differ in the geometry of deeper layers, e.g. by interchanged Ni and Fe atom sites. We considered also systems where the subsurface layer includes both type of atoms.

Results of first principles atomic force minimizations for different models²⁹ can be summarized as follows: the top surface NiFe ordered monolayer is buckled with Fe atoms pushed outwards and Ni atoms pushed inwards. The buckling height in the top surface layer, 0.07 to 0.12 Å, depends on the type of atoms in subsurface layers. We may assume that also in the disordered fcc(001) alloy surface the Fe atoms are pushed outwards and their positions are determined by the local chemical composition of subsurface atoms. The atomically resolved STM images essentially reflect the core positions of the Fe-Ni (001) surface. The brighter spots can be associated with Fe atoms, the darker with Ni atoms. We conclude that the subsurface composition influences the top surface layer buckling as well as the first interlayer distance d_{12} [$d_{12} = d_{12}^{bulk} \pm 2(0.07; +0.02) \text{ Å}$]²⁹. The presence of Ni in the subsurface layer results in a decrease of the first interlayer distance and also the buckling of the surface is smaller. Different local chemical composition in the subsurface explains observed brighter and darker nanometer-sized areas in the measured STM images.

Due to their reduced coordination, surface atoms in magnetic systems have higher magnetic moments as compared to the bulk³¹. It is well known that the surface magnetism depends not only on the coordination number, but also on the details of atomic arrangement. For our models, we have found that their magnetic moments on the surface, 2.97 μ_B for Fe and 0.74 μ_B for Ni, are larger than the bulk values 2.61 μ_B and 0.68 μ_B . The given values are local magnetic moments obtained by integrating the charge distributions over the atomic (muffin-tin) sphere. The calculated work function for the alloy is 4.50 eV.

B. Surface electronic structure

The peak in the tunneling conductivity found about 0.35 eV below the Fermi level seems to indicate that a surface state or a surface resonance exists on the Fe₆₄Ni₃₆ fcc(001) surface at this energy. In order to investigate the surface electronic structure, the spin-polarized local density of states (LDOS) has been calculated for different surface geometries with FP-LAPW. We found a surface resonance below the Fermi level, but its energy and intensity was strongly dependent on the detailed film composition. We needed thick film models (more than 30 layers) to achieve well-converged results, rendering the computational demand for FP-LAPW too high.

Therefore we have applied the tight-binding linear muffin-tin orbital method (TB-LMTO) in the atomic sphere approximation (ASA) to evaluate the surface alloy features. The TB-LMTO code is based on the surface Green function formalism and incorporates realistic boundary conditions. The exchange-correlation potential due to Vosko, Wilk, and Nusair²⁷ has been employed. The dipole barrier effects due to charges spilling out from

the sample into the vacuum are included in the formalism. The effect of randomness in the sample is described in the framework of the CPA (coherent potential approximation), which is able to treat arbitrary concentration profiles close to the sample surface. For further details see Refs. 32 and 33.

The sample consists of two semi-infinite regions, the vacuum and the substrate, sandwiching the intermediate region which also includes few 'substrate' and 'vacuum' layers. The potentials in the intermediate region are determined selfconsistently while for the semi-infinite substrate bulk potentials are used. The vacuum region is represented by a flat potential; and the substrate is a binary alloy Fe₆₄Ni₃₆. The intermediate region consists of 10 atomic layers, namely of three empty-sphere layers adjacent to the vacuum region, two surface alloy layers in which the composition can differ from that in bulk alloy, and five alloy layers in which we assume Invar bulk composition. In this way, charge densities in the intermediate region smoothly match those in the vacuum and substrate regions. The so-called principal layers^{32,33} consisted of two atomic layers. The notation Fe_xNi_{1-x} = Fe_yNi_{1-y} = Fe_{0.64}Ni_{0.36} will be used to describe the composition of the two surface layers. We assume an ideal fcc lattice with a lattice constant of $a = 3.58 \text{ Å}$ for all layers. Thus, no lattice or layer relaxations are assumed. Changes of the interatomic distances due to the surface relaxation are only within few percent and do not affect the electronic structure of the Fe₆₄Ni₃₆ alloy substantially. The buckling of Fe and Ni atoms is also neglected. Possible errors introduced by this approximation become small for Fe-rich alloy surfaces which are of interest here.

The largest contribution to the tunneling current between the tip and the sample comes from the regions around the point $k_k = \frac{\pi}{a}$ of the surface Brillouin zone, where the corresponding k_k -resolved local density of electron states at given energy tends to decay most slowly into the vacuum (cf. eg. Ref. 9). Consequently, we start to analyze the spin- and k_k -resolved local density of states, also called the Bloch spectral function (BSF), evaluated at the tip apex position for $k_k = \frac{\pi}{a}$.

The BSF for a pure iron surface layer on the Fe₆₄Ni₃₆ alloy is shown in Fig. 3. The results clearly demonstrate that a surface resonance appears on iron-rich surfaces in an energy range centered at -0.3 eV, in good agreement with the experimental data. This surface resonance is formed by minority-spin electron states in the central part of the surface Brillouin zone and it has predominantly d_{z^2} character. The totally symmetric A_1 -component of the BSF is also shown. This A_1 -component can be as well expressed as a sum of the s , p_z , and d_{z^2} orbital-resolved components. It is this particular component that gives rise to the surface resonance. The totally symmetric component is expected to decay into the vacuum more slowly than the other components at the same energy do, and this behavior is indeed observed. Let us note that the A_1 -component remains nonzero in the same

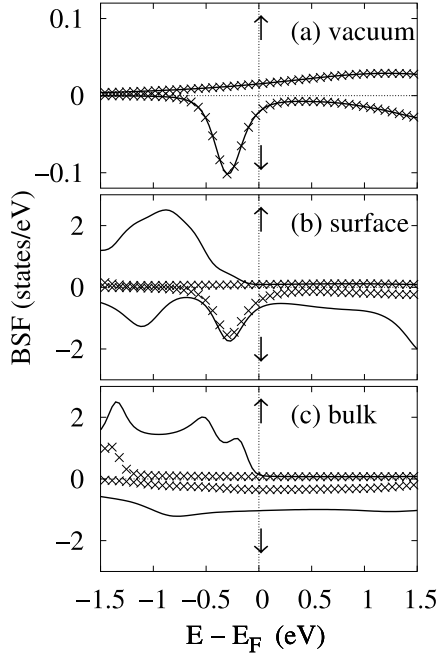


FIG. 3: Solid lines: Layer- and spin-resolved Bloch spectral functions at for $\text{Fe}=\text{Fe}_{0.64}\text{Ni}_{0.36}$ (a) in vacuum 3.6 Å above the surface, (b) in the top surface layer, and (c) in a layer deep in the bulk. Crosses denote the A_1 -symmetry component of the BSF.

energy range also inside the bulk substrate, as shown in Fig. 3 (c). The resonant electron states on the surface can thus hybridize with corresponding bulk states.

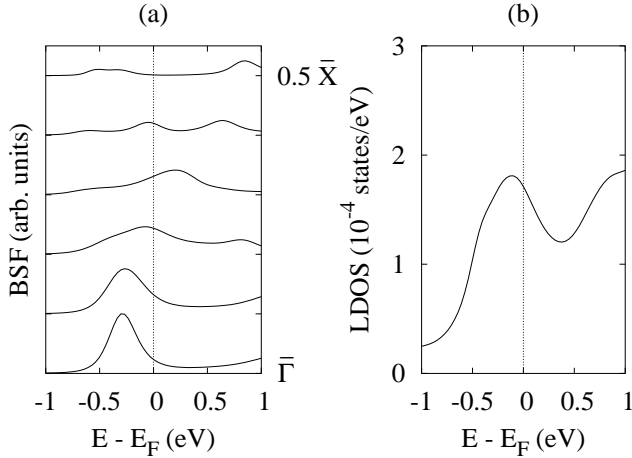


FIG. 4: (a) Minority-spin Bloch spectral functions in vacuum 5.4 Å above the $\text{Fe}=\text{Fe}_{0.64}\text{Ni}_{0.36}$ surface. The BSF is plotted for different k_k -vectors along the path from $k_k = (0;0)$ (bottom) to $k_k = 0.5\bar{X}$ (top). The curves are shifted vertically according to their corresponding k_k -vectors. (b) Local density of states in vacuum 5.4 Å above the $\text{Fe}=\text{Fe}_{0.64}\text{Ni}_{0.36}$ surface.

The energy dispersion of the surface resonance at the iron-covered surface is illustrated in Fig. 4 (a). The

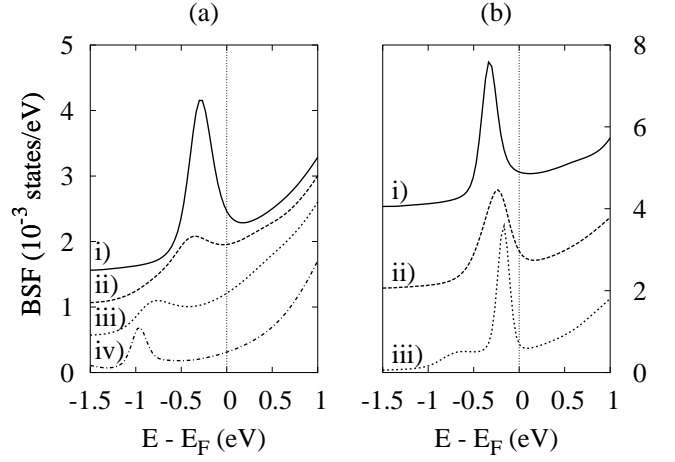


FIG. 5: Bloch spectral functions in vacuum 5.4 Å above the surface. (a) The top surface layer composition is changed: i) $\text{Fe}=\text{Fe}_{0.64}\text{Ni}_{0.36}$, ii) $\text{Fe}_{0.75}\text{Ni}_{0.25}=\text{Fe}_{0.64}\text{Ni}_{0.36}$, iii) $\text{Fe}_{0.50}\text{Ni}_{0.50}=\text{Fe}_{0.64}\text{Ni}_{0.36}$, and iv) $\text{Ni}=\text{Fe}_{0.64}\text{Ni}_{0.36}$. (b) The subsurface layer composition is changed: i) $\text{Fe}=\text{Fe}_{0.64}\text{Ni}_{0.36}$, ii) $\text{Fe}=\text{Fe}_{0.50}\text{Ni}_{0.50}=\text{Fe}_{0.64}\text{Ni}_{0.36}$, and iii) $\text{Fe}=\text{Ni}=\text{Fe}_{0.64}\text{Ni}_{0.36}$. The curves are shifted vertically in order to be better distinguishable.

surface resonance, well resolved at $k_k = 0$, exhibits strong dispersion along the \bar{X} direction in the two-dimensional Brillouin zone. The LDOS is simply the corresponding k_k -integrated BSF and it is shown in Fig. 4 (b). The LDOS reproduces again a pronounced peak for a low binding energy but its position is slightly shifted upwards. This result follows from the fact that contributions from the whole surface Brillouin zone are included in the LDOS on equal footing. The sharp peak observed in the STS experiment indicates that the tip apex acts in this case as a sharp $k_k = 0$ -filter. The contributions from the central part of the surface Brillouin zone dominate. The broadening effects caused both by the energy dispersion of the surface resonance and the tip-sample interaction (not included in our analysis) are more important for small tip-sample distances (below 5 Å)⁹.

The concentration dependence of the surface resonance is shown in Fig. 5 (a). The strength of the surface resonance is reduced with increasing content of Ni-atoms in the topmost surface layer: it almost disappears for less than 75 % Fe in the surface layer. Another surface resonance is formed on the Ni-rich surfaces. This resonance is shifted to lower energies (about 1 eV below the Fermi level) and also corresponds to d_{z^2} -like minority-spin states. We have also explored how the surface resonance on the iron-rich surfaces depends on subsurface composition of the sample [see Fig. 5 (b)]. It turns out that the energy position of the surface resonance depends only weakly on the composition of the subsurface layer. We can conclude that the position of the surface resonance in the spectra is primarily determined by the composition of the topmost layer and, thus, a good indicator

for the local concentration in this layer. This confirms the experimental observations.

IV. CONCLUSION

The chemical contrast in atomically resolved STM images of fcc Fe-Ni alloy surfaces can be explained by *ab initio* calculations which show that the (001) surface of $\text{Fe}_{64}\text{Ni}_{36}$ is buckled: Fe atoms are shifted outwards; Ni atoms inwards. We find that although the surface Fe concentration is 59%, the surface is mostly $c(2 \times 2)$ ordered, which accommodates only 50% Fe. The excess Fe atoms are inserted in frequent very short Fe-rich anti-phase domain boundaries.

In contrast to surface alloys based on a homogeneous bulk, however, the particular distribution of subsurface Fe and Ni atoms additionally modulates the apparent height of the surface atoms in the STM images. Compared to other alloys, this effect is rather strong on the $\text{Fe}_{64}\text{Ni}_{36}$ (001) surface, suggesting significant deviations from a random subsurface distribution, e.g., a decomposition into regions with 50% Fe and 100% Fe similar to the structure of the surface monolayer.

We have also observed a distinct peak in differential tunneling conductance spectra at a negative sample bias of roughly 0.35 eV. However, this peak is strong only in rather small regions on the surface. On the basis of our *ab initio* electronic structure calculations, we attribute this peak to a d_{z^2} -derived surface resonance band that is formed at the Γ -point of the surface Brillouin zone and in its close vicinity with its lower edge 0.3 eV below the

Fermi level. The resonance occurs in model surfaces with high Fe content (75% and more in the topmost layer) and therefore indicates regions on the surface which are Fe enriched, e.g., the mentioned Fe-rich domain boundaries of the $c(2 \times 2)$ ordered surface.

These results show that with certain limitations both surface and subsurface chemical information can be extracted from STM and STS images of the $\text{Fe}_{64}\text{Ni}_{36}$ (001) surfaces: (1) Constant current images with atomic resolution at very low tunneling voltages provide chemical contrast in an atom-by-atom fashion, which, however, is mixed with a height modulation corresponding to the subsurface composition. (2) Constant current images at high, in particular positive, tunneling voltages, which are less sensitive to the surface resonance intensity, map an apparent height, which is a combined effect of the composition of the topmost two or even more monolayers. (3) Current images at voltages just below the surface resonance peak, which are very sensitive to the surface resonance intensity, show the surface composition with a lateral resolution on the nanometer scale without significant interference by the subsurface composition.

Acknowledgments

This work has been done within the project AVO Z10100520 of the ASCR. The financial support provided by the Academy of Sciences of the Czech Republic (Grant No. A1010214) and by the FWF (Austrian science fund) is acknowledged.

Electronic address: m.aca@fzu.cz

^y Present address: Institute of Materials Science and Technology, Vienna University of Technology, Favoritenstrasse 9-11, 1040 Vienna, Austria

¹ M. Schmid, H. Stadler, and P. Varga, *Phys. Rev. Lett.* **70**, 1441 (1993).

² M. Schmid and P. Varga, in *Alloy Surfaces and Surface Alloys*, ed. D. P. Woodruff, Elsevier, Amsterdam (2002), p. 118-151.

³ E. L. D. Hebenstreit, W. Hebenstreit, M. Schmid, and P. Varga, *Surf. Sci.* **441**, 441 (1999).

⁴ P. T. Wouda, B. E. Nieuwenhuys, M. Schmid, and P. Varga, *Surf. Sci.* **359**, 17 (1996).

⁵ D. D. Chambliss and S. Chiang, *Surf. Sci.* **264**, L187 (1992).

⁶ C. Nagl, O. Haller, E. Platzgummer, M. Schmid, and P. Varga, *Surf. Sci.* **321**, 237 (1994).

⁷ L. P. Nielsen, F. Besenbacher, I. Stensgaard, E. Laegsgaard, C. Engdahl, P. Stoltze, K. W. Jacobsen, and J. K. Nørskov, *Phys. Rev. Lett.* **71**, 754 (1993).

⁸ M. F. Crommie, C. P. Lutz, and D. M. Eigler, *Nature* **363**, 524 (1993).

⁹ J. A. Stroscio, D. T. Pierce, A. Davies, R. J. Celotta, and M. Weinert, *Phys. Rev. Lett.* **75**, 2960 (1995).

¹⁰ W. A. Hofer, J. Redinger, A. Biedermann, and P. Varga, *Surf. Sci.* **482-485**, 1113 (2001).

¹¹ A. Davies, J. A. Stroscio, D. T. Pierce, and R. J. Celotta, *Phys. Rev. Lett.* **76**, 4175 (1996).

¹² A. Biedermann, O. Genser, W. Hebenstreit, M. Schmid, J. Redinger, R. Podlucky, and P. Varga, *Phys. Rev. Lett.* **76**, 4179 (1996).

¹³ M. M. J. Bischof, C. Konvicka, A. J. Quinn, M. Schmid, J. Redinger, R. Podlucky, P. Varga, and H. van Kempen, *Phys. Rev. Lett.* **86**, 2396 (2001); *Surf. Sci.* **513**, 9 (2002).

¹⁴ J. Tersoff and D. R. Hamann, *Phys. Rev. B* **31**, 805 (1985).

¹⁵ M. Posternak, H. Krakauer, A. J. Freeman, and D. D. Koelling, *Phys. Rev. B*, **21**, 5601 (1980).

¹⁶ A. Rehbein, D. Wegner, G. Kaindl, and A. Bauer, *Phys. Rev. B* **67**, 033403 (2003).

¹⁷ M. van Schilfegaarde, I. A. Abrikosov, and B. Johansson, *Nature* **400**, 46 (1999).

¹⁸ J. L. Robertson, G. E. Ioe, C. J. Sparks, X. Jiang, P. Zschack, F. Bley, S. Lefebvre, and M. Bessiere, *Phys. Rev. Lett.* **82**, 2911 (1999).

¹⁹ P. Entel, E. Homann, P. Mohn, K. Schwarz, and V. L. Monuzzi, *Phys. Rev. B* **47**, 8706 (1993).

²⁰ P. Mohn, K. Schwarz, and D. Wagner, *Phys. Rev. B* **43**, 3318 (1991).

- ²¹ R. F. W illis and N. Janke-G ilm an, *Europhys. Lett.* 69, 411 (2005).
- ²² V. C risan, P. Entel, H. Ebert, H. A kai, D. D. Johnson, and J. B. Staunton, *Phys. Rev. B* 66, 014416 (2002).
- ²³ T. H anke, M. Bode, S. K rause, L. Berbil-Bautista, and R. W iesendanger, *Phys. Rev. B* 72, 085453 (2005).
- ²⁴ M. F. C rom m ie, C. P. Lutz, and D. M. E igler, *Phys. Rev. B* 48, 2851 (1993).
- ²⁵ M. W einert, E. W im m er, and A. J. Freeman, *Phys. Rev. B* 26, 4571 (1982); see also <http://www.apw.de>.
- ²⁶ URL: <http://www.uwm.edu/~weinert/air.html>.
- ²⁷ S. H. Vosko, L. W ilk, and M. Nusair, *Can. J. Phys.* 58, 1200 (1980).
- ²⁸ J. P. Perdew, K. Burke, and M. Ernzerhof, *Phys. Rev. Lett.* 77, 3865 (1996).
- ²⁹ M. Ondracek, F. M aca, J. Kudmovsky, and J. Redinger, *Czech. J. Phys.* 56, 69 (2006).
- ³⁰ A. P. M iodownik, *J. Magn. Magn. Matter.* 10, 126 (1979).
- ³¹ A. J. Freeman and R. W u, *J. Magn. Magn. Mater.* 100, 497 (1991).
- ³² J. Kudmovsky, I. Turek, V. D rchal, P. Weinberger, S. K. Bose, and A. Pasturel, *Phys. Rev. B* 47, 16525 (1993).
- ³³ I. Turek, V. D rchal, J. Kudmovsky, M. Sob, and P. Weinberger, *Electronic Structure of Disordered Alloys, Surfaces and Interfaces*, K luwer Academic Publishers, Boston (1997).